Sodium-MRI using a density adapted 3D Radial Acquistion Technique

A. M. Nagel[1], F. B. Laun[1], M-A. Weber[2], C. Matthies[1], W. Semmler[1], and L. R. Schad[3]

[1]Medical Physics in Radiology, German Cancer Research Center, Heidelberg, Germany, [2]Department of Diagnostic and Interventional Radiology, University Hospital Heidelberg, Heidelberg, Germany, [3]Computer Assisted Clinical Medicine, University Heidelberg, Mannheim, Germany

Introduction

Due to the fast transversal relaxation [1], pulse sequences that enable short echo times like 3D projection reconstruction (3DPR) [2] and twisted projection imaging (TPI) [3] are favorable for sodium imaging. 3DPR is often preferred due to the straightforward, convenient form of the k-space trajectory, but suffers from a reduced SNR efficiency [4]. In this work we propose a pulse sequence that combines both, the convenience and flexibility of 3DPR and the enhanced SNR efficiency of TPI. A pulse sequence based on a conventional 3DPR sequence was adapted such that the sampling density in the outer part of k-space is kept constant (DA-3DPR). This optimized pulse sequence is compared with a 3DPR sequence and the differences are elucidated in simulations and both in phantom and *in vivo* measurements.

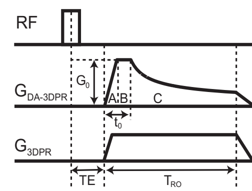

Fig. 1. Sampling scheme of the two 3D sequences 3DPR and DA-3DPR.

Methods

A 3DPR and a DA-3DPR pulse sequence were implemented on a 3.0 T clinical whole-body MR system (Magnetom Tim Trio, Siemens Medical Solutions, Erlangen, Germany). The readout gradient shapes of both sequences are schematically shown in Fig. 1. Due to the falling gradient amplitude the DA-3DPR sequence achieves a higher homogeneity in the sampling density. Thus the image noise is decreased.

A phantom containing cavities to generate image contrast is employed to compare the two sequences. Additionally, an analytical phantom of the same geometry as the real phantom was computed in k-space. The degradation of image quality due to noise and the influence of B_0-inhomogeneities were simulated for both sequence designs. Parameters: $T_{RO} = 10$ ms; $\Delta\nu = 0$ Hz (32 Hz; 64 Hz); 14000 projections; 3DPR: G = 1.11 mT/m; DA-3DPR: $G_0 = 9.83$ mT/m; $t_0 = 0.25$ ms.

Due to transversal relaxation, the k-space signal depends on the sampling scheme. To quantify the resulting blurring and loss of signal, the point-spread functions $P_{tot}(x)$ (PSF) were simulated for different ratios of T_{RO}/T_2^*. The blurring was quantified by the full width at half maximums (FWHM) of the PSFs and the SNR by $\sqrt{T_{RO} P_{tot}(0)}$.

To evaluate the performance of the sequences, brain images were acquired. The influence of the readout length T_{RO} was investigated by acquiring data sets with $T_{RO} = 5$ ms, 10 ms, 20 ms, 30 ms and 40 ms. Parameters: TR = 50 ms, TE = 0.2 ms, $\alpha = 77°$, 13000 projections, 1 average, voxel size: 4x4x4 mm^3.

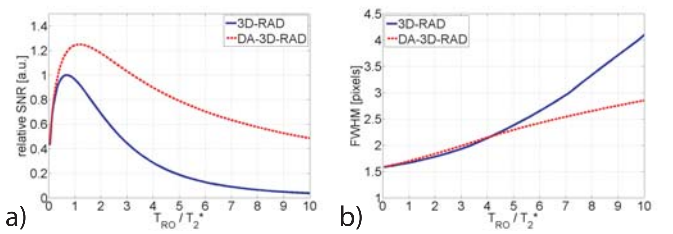

Fig. 2. a) Relative SNR as a function of the readout duration T_{RO}. b) FWHM of the PSFs.

Results

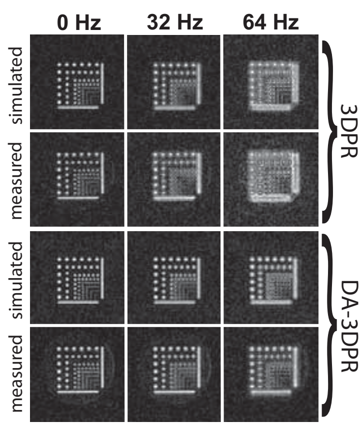

Fig. 3. Simulations and phantom measurements investigating the effect of field inhomogeneities.

The optimal readout window, for which the SNR is maximal, is $T_{RO} = \alpha T_2^*$, with $\alpha = 0.69$ for trapezoidal gradients and $\alpha = 1.18$ for density adapted gradients considering hardware limitations (Fig. 2a). The corresponding SNR gain is 1.25 compared to conventional radial sampling (Fig. 2a). This gain in SNR is solely caused by the more efficient signal acquisition with respect to T_2^* decay. Further considering the gain due to the more homogeneous sampling density, which is approximately a factor 1.32 (calculation in analogy to [4] (not shown)), a total benefit of 1.66 can be obtained. The FWHMs of the PSFs mainly coincide for all sampling schemes if $T_{RO} < 4T_2^*$ (Fig. 2b). For longer readout intervals, the FWHM of the 3DPR sequence is significantly higher, indicating a strong blurring.

Fig. 3 shows the effect of frequency offsets on image quality. Blurring markedly degrades image quality for conventional 3D radial sampling at 32 Hz frequency offset (1 ppm at $B_0 = 3$ T). However, using the density adapted sampling, the blurring is negligible for 32 Hz frequency offset and it is also markedly reduced at 64 Hz offset. The agreement between simulations and experiments is convenient.

In vivo brain images are shown in Fig. 4. The DA-3DPR sequence provides a higher SNR in the unfiltered images (Fig. 4a). SNR values for ROI's in the eyes and in brain tissue are shown in Fig. 5. For all readout window lengths, DA-3DPR sampling shows a significantly higher SNR. The differences in SNR are more pronounced in brain tissue than in the eyes. Although the SNR benefit is lost when Hanning filtering is used, the acquisition with the DA-3DPR sequence still yields a better resolution and less blurring (Fig. 4b).

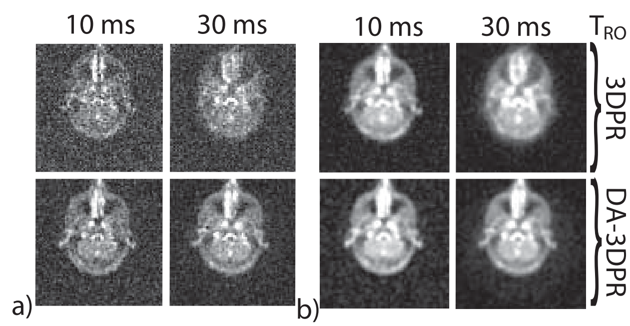

Fig. 4. Images of 3D ^{23}Na brain data sets. a) Images were reconstructed without filtering. b) The images that are shown in (a) were reconstructed applying a Hanning filter.

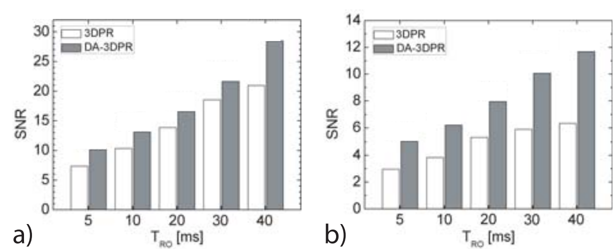

Fig. 5. SNR values of the images shown in Fig. 4a, b and images that were acquired with other readout lengths. a) SNR in the eyes. b) SNR in brain tissue.

Discussion

The density adapted sampling provides significantly increased SNR. The optimal readout length is hard to identify since the sodium transversal relaxation times vary over a broad range in biological tissue. Here, the DA-3DPR sampling provides good SNR in contrast to conventional 3DPR sampling even for readout times that deviate significantly from the optimal time (Fig. 2). This becomes apparent in the *in vivo* brain images (Fig. 4). In regions with short transversal relaxation times, as in brain tissue, the benefit of DA-3DPR is larger than in compartments with longer T_2^* relaxation times such as liquor or eyes. Furthermore, with higher field strengths B_0, inhomogeneities increase and the benefits of density adapted sampling regarding blurring artifacts might become even more pronounced. The straightforward form of the radial trajectory further enables a flexible sequence design and is therefore a well suited alternative to the more complicated TPI trajectories.

References

[1] Constantinides et al.; Radiology (2000); 216: 559-568
[2] Nielles-Vallespin et al.; MRM (2007); 57: 74-81
[3] Boada et al.; MRM (1997); 37: 706-715
[4] Liao et al.; MRM (1997); 37: 569-575
[5] Bartha and Menon; MRM (2004) ; 52: 407-410